Performance Evaluation of Unidirectional Molds used for Measuring Saturated Transverse Permeability of Engineering Textiles

Bin Yang[a,b], Yixun Sun[b], François Trochu[b], Cédric Béguin[b], Jihui Wang[a], Philippe Causse[c*]

[a] School of Material Science and Engineering, Wuhan University of Technology, 122 Luoshi Road, Hongshan, 430070 Wuhan, PR China
[b] Department of Mechanical Engineering, Research Center for High Performance Polymer and Composite Systems, Polytechnique Montréal, 2900 Boulevard Edouard Montpetit, Montréal, Québec H3T 1J4, Canada
[c] Department of Mechanical Engineering, École de Technologie Supérieure (ETS), 1100, rue Notre-Dame Ouest, Montréal, Québec H3C 1K3, Canada

*Corresponding Author: philippe.causse@etsmtl.ca

Abstract

Transverse permeability measurement of engineering textiles by state-of-the-art approaches revealed considerable discrepancies between different test devices. The absence of performance analysis protocols makes quantifying error sources challenging. This work addresses this issue by providing approaches for evaluating performance of unidirectional test devices and obtaining transverse permeability from conventional saturated tests. Firstly, experiments are presented to illustrate how flow distribution plates affect flow capacity and lead to underestimation of permeability. To quantify this effect and describe device performance, a dimensionless descriptor, discharge coefficient, is introduced. The latter appears to depend on mold geometry and sample thickness and anisotropy. An iterative framework is then established to obtain intrinsic transverse permeability through simulations or using the descriptor. Two molds were investigated with actual textiles. The first underestimated permeability by up to 51%, whereas the second by 36%, resulting in inconsistency. Comparatively, the proposed approach significantly improved measurement accuracy and consistency for both molds.

Keywords: Engineering textiles; Transverse permeability; Mold performance; Iterative framework

1. Introduction

In sectors such as automotive, low-cost, high-volume production is key for textile reinforced thermoset and thermoplastic composites to find practical applications, but achieving defect-free fabrication is technologically challenging. Transverse impregnation plays a key role in efficiently manufacturing

composites by modern *Liquid Composite Molding* (LCM) techniques because it provides a much shorter flow path than in-plane directions [1, 2]. Hence, it is of high practical significance to determine the capability of textile reinforcements in establishing through-thickness flow. This is quantified by transverse permeability according to Darcy's law [3]:

$$\vec{u} = -\frac{\overline{\overline{K}}}{\mu\phi} \cdot \vec{\nabla} p \tag{1}$$

where $\overline{\overline{K}}$ is the permeability tensor (m^2) depending on fabric architecture and fiber volume fraction, $\vec{u}$ is the physical velocity of the test fluid (also known as intrinsic average velocity [4], $\mathrm{m/s}$), ϕ is the porosity of specimen, μ is the dynamic viscosity of fluid in $\mathrm{Pa \cdot s}$ and p fluid pressure in Pa. A survey conducted by the National Physical Laboratory in 2016 confirmed the interest in standardizing the transverse permeability measurement [5].

Methods developed to determine the transverse permeability of engineering textiles fall primarily into two categories. The first category, referred to as unidirectional method or 1D method, involves establishing a quasi-unidirectional through-thickness flow across a fibrous preform sandwiched between two rigid flow distribution plates (e.g., perforated plate [6-9], aluminum honeycomb [10] and porous media [11]). The transverse permeability can be determined knowing the pressure gradient and liquid flow rate. Typically, the test mold is cylindrical (see Fig. 1) [7, 8, 12, 13]. Few investigations used square molds [14], or special devices to continuously alter the compaction level of textile samples [15, 16]. A number of devices also integrated sample thickness [8, 17] and textile layer position [9] tracking systems to evaluate the effect of hydrodynamic compaction [13] induced by injection pressure of the test liquid.

The second category includes various 3D methods that relate the principal permeability with the flow front position of a 3D transient flow through a textile specimen [18-21]. The permeability tensor can be obtained in this case either analytically by solving governing equations [20, 22] or numerically by matching the actual flow front on a case-by-case basis [21, 23]. Due to the complexity in flow front tracking and data analysis, 22 out of the 28 tests reported by 26 participants in an international benchmarking project (hereafter referred to as Benchmark III) [24] were obtained by the unidirectional approach with saturated flow conditions.

Transverse permeability measurement remains challenging, as evidenced by results of Benchmark III: experimental results obtained with the same textiles showed differences of about two orders of magnitude. Even after excluding the possible outliers, the maximum value was still roughly four times larger than the minimum. In spite of this, the single-factor analysis failed to identify any significant error sources [24]. The challenges are primarily caused by the following two aspects:

One is connected with the test mold, data analysis, and operational guidelines. Among them, a fully calibrated test mold forms the basis for a more extensive error source analysis. Research [7, 25] demonstrated that flow distribution plates in 1D molds may lead to permeability underestimation since they alter flow path and reduce mass transfer efficiency. Neither experimental evidence of the underestimation nor a method for 1D mold calibration has been published to date. This makes it difficult to quantify the efficiency of test molds.

The other is related to the material. The inherent variability of materials, partly caused by manual handling, dual-scale structure [26] and layer nesting [27, 28] are well-known factors that contribute to the inconsistency between measurements. Besides, the deformable nature of engineering textiles makes rigid sample holders necessary to maintain fiber volume fraction. As a result, in-plane flow is introduced. The specimen permeability anisotropy and thickness may play a role in this case [7]. Furthermore, microstructure variations may also appear due to flow-induced compaction [8, 9, 13].

Therefore, it is imperative to determine the efficiency of a 1D test mold for mass transfer to improve measurement accuracy. It is usually related to the cross-sectional area of test molds or the open space of flow distribution plates. For instance, Merhi et al. [10] described a transverse permeability test in which the fiber bed (140 mm in diameter) was sandwiched between two distribution plates of 100 mm in diameter. For permeability calculations, the area of the plates, rather than the sample area, was used as an estimation of the limited flow transfer capability. Similar approximation was also adopted by Huang et al. [6], Swery et al. [29], and Studer et al [30]. A rigorous theoretical analysis is, however, required for accurate assessment. Furthermore, the flow exchange capability may also vary depending on the specimen, as will be demonstrated in this study.

The current work aims to improve the accuracy and reproducibility of the conventional 1D method by quantifying and correcting the effect of test devices on the measured transverse permeability. The paper is organized as follows: experimental evidence is first presented in Section 2 to illustrate the issues associated with conventional 1D test methods. A dimensionless number, discharge coefficient, is introduced as a performance descriptor to assess mold efficiency. Section 3 presents a numerical procedure for building the characteristic performance map of a test mold. In Section 4, we propose a method for determining intrinsic permeability from conventional 1D measurements for isotropic materials based on the performance descriptor. Section 5 extends the method to anisotropic materials and validation experiments are conducted with a fibrous textile. Finally, the approach is applied to investigate the discrepancy in permeability tested by two different unidirectional molds in Section 6.

2. Evidence for permeability underestimation of the conventional 1D method

2.1 Equipment and method

Permeability tests were conducted with an existing unidirectional testing device (see Fig. 2a) that was previously used for Benchmark III. The specimen was held between a pair of 6.5-millimeter-thick metallic flow distribution plates. As shown in Fig. 2b, the perforations in the plates are arranged in a hexagonal pattern and are not present near the edges of the plate. This leads to an open space ratio (γ_p) of 35.1%. The testing fluid enters the mold from the bottom inlet at a controlled flow rate and leaves from the top at atmospheric pressure. Injection pressure is monitored by sensors on the bottom of the mold. The testing fluid was XIAMETER® PMX-200 100cst silicone oil (density 964 $\mathrm{kg/m^3}$). Its viscosity μ (Pa·s) was determined using Eq. (2) obtained by fitting experimental results against temperature T:

$$\mu = 0.001e^{6.061}T^{-0.473}, 21\,℃ < T\,(℃) < 26\,℃ \tag{2}$$

The apparent transverse permeability K_z^a was computed according to Darcy's law from the measured pressure drop ΔP (Pa) and liquid volume flow rate Q ($\mathrm{m^3/s}$):

$$K_z^a = \frac{Q}{A} \cdot \frac{h\mu}{\Delta P} \tag{3}$$

where A (m^2) is the mold cavity cross-sectional area (area of the perforated plates) and h (m) the sample thickness controlled by distance between two flow distribution plates. The equivalent permeability of the flow distribution plates K_p was estimated using the model derived [31] based on Hagen-Poiseuille relation:

$$K_p = \frac{n_h \pi R^4}{8A} \quad (4)$$

where n_h is the number of the holes, R the hole radius. K_p can thus be estimated as 6.2×10^{-7} m^2, between 3 and 5 orders of magnitude higher than typical textile reinforcements. This indicates that additional pressure drop caused by the perforated plates is negligible. It agrees with the report of Barnett et al. [16], although it may need to be considered in some limiting cases (extremely low thickness or high permeability).

2.2 Permeability of reference porous medium

A reference isotropic porous medium made of sintered ceramic balls of 0.2 mm diameter (Fig. 3a) was tested with the unidirectional mold to quantify the mold performance. It has the advantage of being much more rigid than engineering textiles. This allowed comparing the results obtained with and without flow distribution plates, as depicted in Fig. 3. The transverse permeability measured with perforated plates (Fig. 3b) is referred to as apparent permeability K_z^a, which can be influenced by a deviation from unidirectional flow caused by the plates. In comparison, the value measured in freestanding condition (Fig. 3c) is referred to as the intrinsic permeability K_z, since a quasi-unidirectional flow satisfying 1D Darcy's law can be established in this case.

Two specimens of the reference porous medium with different thicknesses, 11.6 mm and 25 mm, were tested. The samples were machined to a diameter of 94.5 mm. The gap between the specimen and the mold wall was sealed to prevent any edge effect. Each sample was tested with and without distribution plates. Experimental results are reported in Fig. 4. In each case, an almost perfectly linear relationship between flow rate and pressure drop ($R^2 \sim 0.999$) is observed. This confirms that possible unfavorable effects, such as flow-induced compaction and nesting effect, were avoided. The presence of the perforated plates can then be considered the only important factor in analyzing experimental results and evaluating the testing procedure.

Permeability is an intrinsic property that should not depend on the operational conditions of measurements. However, the values reported in Table 1 for the reference material contradict this concept in two aspects:

1) The apparent permeability is specimen thickness sensitive. Significant inconsistency (18%) in apparent permeability was observed for specimens of different thickness. In comparison, the intrinsic permeability is in good agreement (the 4% difference is possibly induced by machining).

2) The presence of flow distribution plates leads to considerable permeability underestimation. As expected from the difference in pressure drop (Fig. 4), the intrinsic permeability is 43% and 26% higher than the corresponding apparent permeability for the thinner and thicker specimens, respectively.

The underestimation could be caused by (1) additional pressure drop through the perforated plates and (2) limited fluid exchange capacity between the specimen and the free flow zone due to perforated plates. As the pressure drop associated with the devices is negligible, the second one becomes critical for accurate permeability characterization. It is, however, necessary to use flow distribution plates as holders since actual textiles are deformable and compressible. In the following, the impact of the plates on the measurement will be quantified numerically to eventually propose a correction strategy.

2.3 Performance of unidirectional molds

A performance descriptor named the discharge coefficient C_{d} is introduced to evaluate the flow capacity and performance of unidirectional molds. It is simply computed as the ratio of the apparent discharge Q^a (m^3/s) measured through a given test mold with flow distribution plates to the theoretical discharge $Q^{1\mathrm{d}}$ for unidirectional Darcy flow at the same pressure gradient:

$$C_{\mathrm{d}} = \frac{Q^a}{Q^{1\mathrm{d}}} = \frac{K_z^a}{K_z} \tag{5}$$

The above definition is thus equivalent to $K_z = K_z^a / C_{\mathrm{d}}$, considering C_{d} as a correction factor to obtain the intrinsic permeability from the apparent permeability. With the measurement data on the reference material, the corresponding discharge coefficient C_d of 69% and 79% can be obtained for the thinner and the thicker specimens, respectively. It should finally be noted that for any similar test mold, the discharge coefficient takes values between 0 and 1 and is expected to decrease when the open space ratio of the perforated plates is reduced. As will be shown later, the discharge coefficient is not a constant for a specific device but also depends on characteristics of the porous sample.

3. Numerical characterization of 1D experimental setup

3.1 Motivation

The motivation of this research is to establish a robust approach to obtain intrinsic permeability while maintaining the advantages of the conventional method (e.g., inexpensive, simplicity of data processing and sample preparation). The method consists of quantitatively evaluating the performance of test devices by computing the discharge coefficient using numerical simulation. The unidirectional flow rate is calculated using Darcy's law while the apparent flow rate Q^a is predicted using numerical simulation. The latter is detailed in this section. In Sections 4 and 5, the method is then applied to predict the characteristic performance map of 1D molds and identify the intrinsic transverse permeability from apparent measurements.

3.2 Governing equations

The numerical domain consists of two solid-free subdomains (upstream and downstream) and a porous zone representing the fibrous preform, as illustrated in Fig. 5. Assuming constant porosity ϕ and single phase flow, the volume-averaged mass and momentum conservation equations for flow in porous media are as follows:

$$\nabla \cdot (\rho \vec{u}) = 0 \tag{6}$$

$$\nabla \cdot (\rho \vec{u}\vec{u}) = -\vec{\nabla} p + \nabla \cdot \mu \left[\left(\vec{\nabla}\vec{u} + \vec{\nabla}\vec{u}^{\mathrm{T}} \right) - \frac{2}{3} \nabla \cdot \vec{u} \bar{\bar{I}} \right] + \rho \vec{g} - \left(\bar{\bar{K}}^{-1} \phi \mu \vec{u} + \frac{\phi^2 C_2}{2} \rho |\vec{u}| \vec{u} \right) \tag{7}$$

where ρ, μ and $\vec{u}$ are, respectively, the density, viscosity, and intrinsic average velocity of the fluid. p denotes the static pressure, $\bar{\bar{I}}$ the identity tensor and $\vec{g}$ the gravitational acceleration. The last two terms of Eq. (7) in the bracket of the right-hand side describe the viscous and inertial resistance of flow in porous media. In this research, the inertial resistance is neglected ($C_2 = 0$) because of the low Reynolds number ($Re < 1$) for practical resin flow in engineering textiles. Note that in the solid-free subdomain where $\phi = 100\%$ and $\bar{\bar{K}} \to \infty$, Eq. (6) and Eq. (7) reduce to standard Navier-Stokes equations for single phase flow.

3.3 Geometrical model and boundary conditions

The geometrical model and the boundary conditions are also described in Fig. 5. The analysis takes into account the geometrical features of the mold, the thickness, and the permeability anisotropy of the specimen as the flow pattern might be altered by these factors [7]. The dimensions are the same as the device described in Fig. 2. Pressure boundary conditions are assigned to the inlet and outlet. The domain is discretized in a

non-conforming hexahedral-dominated mesh. Mesh sensitivity analysis was conducted by considering different grid resolutions to ensure the independence of the numerical solutions from the mesh size. The mass and momentum conservation equations are discretized by the second-order upwind scheme. The Semi-Implicit Method for Pressure Linked Equations (SIMPLE) algorithm [32] is employed to decouple the pressure–velocity linkage to solve the incompressible flow problem. The convergence criterion was set to be 10^{-5} for all residuals. The simulations were performed with ANSYS Fluent.

The flow is assumed to be Newtonian, isothermal, and incompressible. Besides, previous knowledge of the in-plane permeability of the preform is required to complete the simulation. Nevertheless, it will be shown in Section 5.5 that the numerical results are not sensitive to in-plane permeability with acceptable errors. The other properties needed to run the simulation are viscosity and density of the test fluid.

4. Correction of permeability measurements with isotropic materials

This section presents the use of the discharge coefficient for correcting the permeability of isotropic materials. A parametric study is first conducted to predict the performance of the setup for varying test conditions. The approach is then validated using experimental data previously acquired with the reference porous medium.

4.1 Numerical evaluation of mold performance

The apparent flow rate through an isotropic porous sample was predicted at a constant pressure gradient numerically for permeability ranging from 1E-13 m^2 to 1E-10 m^2, and specimen thickness from 1.5 mm to 60 mm. The corresponding discharge coefficient is reported in Fig. 6 with permeability underestimation Δ_K representing the relative difference between the apparent and intrinsic permeability:

$$\Delta_K = \frac{K_z - K_z^a}{K_z^a} \times 100\% = \frac{1 - C_d}{C_d} \times 100\% \quad (8)$$

It can first be noted that the discharge coefficient does not vary with permeability values, as shown by the superimposed markers corresponding to numerical simulation in Fig. 6. This is not surprising because the pressure drop of the plates is negligible and because the porous sample is isotropic. In that case, the permeability tensor reduces to a scalar and the apparent flow rate Q^a varies linearly with permeability for given pressure difference and sample thickness. Since the theoretical flow rate $Q^{1\mathrm{d}}$ is also proportional to K_z,

the discharge coefficient varies only with the sample thickness as indicated by the trend line. This numerically built performance indicator agrees well with the data points derived from experiments presented in Section 2.3 (red star markers).

Fig. 6 also indicates that the underestimation of transverse permeability can exceed 100% for isotropic specimens with a thickness less than 5 mm. The discharge coefficient increases with specimen thickness as the effect of the perforated plates diminishes and flow tends to get closer to unidirectional conditions. This is consistent with our previous numerical study [7], which showed that apparent permeability could only approach the intrinsic permeability of a specimen when sample thickness exceeds 50 mm. However, such test condition seems impractical for actual fabric characterization due to increased material and time costs.

4.2 Permeability correction and validation

Fig. 7 compares the measured apparent and intrinsic permeability, and the corrected value obtained by applying Eq. (8) with the numerically determined C_d. For the two reference samples, the corrected permeabilities are similar and in quite good agreement with intrinsic values. The largest difference of 4% is observed for the thinner specimen, which may be due to the slightly uneven specimen thickness caused by machining. Overall, results indicate that the apparent permeability measured by the conventional test can be adequately corrected with the C_d performance indicator, demonstrating the validity of the proposed approach.

5. Correction of permeability measurements with orthotropic materials

In this section, the approach for permeability correction is extended to orthotropic materials. We first show that the result of the permeability test is influenced by anisotropy of the sample so that this parameter must be considered when modelling the performance of the mold. Two iterative frameworks are then presented for permeability correction based on the discharge coefficient and validated with tests on a typical fibrous fabric.

5.1 Influence of global permeability anisotropy

Common fibrous preforms exhibit a quasi-orthotropic behavior. If the coordinate system is chosen to coincide with the principal directions of the material, the permeability tensor reads:

$$\boldsymbol{K} = \begin{bmatrix} K_x & 0 & 0 \\ 0 & K_\mathrm{y} & 0 \\ 0 & 0 & K_\mathrm{z} \end{bmatrix} \tag{9}$$

In-plane permeability components K_x and K_y are usually significantly higher than K_z. This is considered by global permeability anisotropy α_g defined as:

$$\alpha_g = \frac{\sqrt{K_x\, K_y}}{K_z} \tag{10}$$

The anisotropic behavior influences the permeability test by altering the flow pattern in the sample. This is shown in Fig. 8b, which plots the intrinsic average velocity magnitude in a cross-section located at the center of the mold (the visualization zone covering one full and two half perforations as shown in Fig. 8a). To obtain these numerical results, the transverse permeability was kept constant (1×10^{-11} m^2) while the in-plane permeability was taken equal ($K_x = K_y$) and selected to achieve the given anisotropy. In all simulations, the pressure gradient across the sample was 2000 Pa/mm. The solid part of perforated plates, which is impermeable, is represented in gray in Fig. 8b.

The four left panels of Fig. 8b were obtained with an isotropic material ($\alpha_g = 1$) and corresponds to results already presented in Fig. 6. As can be seen, the fluid in the porous medium between the impermeable part of the perforated plates is nearly stagnant for the case with the thinnest sample ($h = 1.5$ mm). When the thickness increases, the stagnant zone decreases and a flow redistribution can be observed so that the intrinsic average velocity tends to become uniform in the mid-plane of the sample. For a given preform thickness, increasing global permeability anisotropy facilitates in-plane flow redistribution in the vicinity of the plates and the averaged flow becomes unidirectional more rapidly. In the case of thickest sample and highest global permeability anisotropy ($h = 15$ mm and $\alpha_g = 100$), the intrinsic average velocity field is almost uniform in a large part of the sample and flow conditions are quite close to quasi-unidirectional because the sample itself plays a role of flow distribution media that offsets the limited flow exchange capacity induced by perforated plates. Consequently, the apparent transverse permeability measured with an orthotropic material depends not only on the device but also on the global permeability anisotropy and thickness of the specimen.

5.2 Evaluation of mold performance

Following the approach of Section 4.1, the characteristic performance map of the mold was numerically characterized for a wide range of specimen thickness and global permeability anisotropy. As shown in Fig. 9,

the discharge coefficient for $\alpha_g > 1$ is significantly enhanced compared to isotropic case at the same thickness because higher in-plane permeability facilitates flow redistribution. However, the effect of global permeability anisotropy becomes less noticeable once α_g is greater than 50. Note that the two in-plane permeability components, K_x and K_y, are assumed to be equal. As for the isotropic material, other simulations also confirmed that the discharge coefficient is not affected by the absolute value of transverse permeability if the thickness and anisotropy are same. Besides, a simulation performed with $K_x = 10K_y = 10K_z$ shows that the discharge coefficient is quite similar to the one for $K_x = K_y$ with an error less than 2%. It is then reasonable to consider that Fig. 9 describes the performance of the test device for any orthotropic preform.

A simple analytical model was proposed to relate the performance descriptor C_d to the open space ratio γ_p of a flow distribution plate (with perforations in hexagonal pattern) and the thickness and global permeability anisotropy of the specimen. It is given by:

$$C_d(h,\ \alpha_g) = \frac{(1-\gamma_p)h}{h + \frac{E}{\sqrt{\alpha_g}}} + \gamma_p \tag{11}$$

In this general model, the only unknown E is a constant to be determined by making use of the data obtained from either numerical simulations or experiments. As shown by the dashed lines in Fig. 9, the model represents the predicted discharge coefficient quite precisely (E=13.6, R-square = 0.99). In addition, the model is bounded between the open space ratio of the distribution plate and 1. This is consistent with the fact that when $h \to 0$, the flow can only develop in perforations, whereas it approaches a 1D ideal flow for $h \to \infty$.

5.3 Iterative framework for transverse permeability identification

For anisotropic materials, the discharge coefficient C_d cannot be computed directly since the anisotropy is a priori unknown. To tackle this issue, two iterative frameworks are presented here.

(1) Numerical-based approach

This method consists of running a series of flow simulations for each test. Its principle is rather similar to past work on 3D unsaturated tests that matched simulation results with the experimental flow front to identify the material permeability [21, 23] except it matches the experimental and numerical flow rates. It uses a

numerical model that replicates the test conditions (mold geometry, pressure drop, etc.). The apparent permeability measured by the conventional method is used as initial value for transverse permeability in the first simulation. It is then updated iteratively using Eq. (12) to minimize the residual R_{nu}:

$$K_{z,i+1} = \frac{Q_{exp}}{Q_i} \times K_{z,i} \tag{12}$$

$$R_{nu} = \frac{Q_{exp} - Q_i}{Q_{exp}} \times 100\% \tag{13}$$

where Q_{exp} is the experimental flow rate, Q_i is the flow rate predicted by simulation and i stands for the i-th iteration. The output (when $R_{nu} < 0.5\%$) is referred to as numerically identified permeability to distinguish from intrinsic transverse permeability measured directly by experiment. This strategy is summarized below:

Algorithm 1: Numerical based approach

Input : P_{in}, P_{out}, K_x, K_y, K_z^a
Output : K_z^{nu}
K_x, $K_y \leftarrow$ in-plane permeability;
$K_z \leftarrow K_z^a$;
Read full-scale numerical mesh;
Impose boundary conditions P_{in} and P_{out};
while *True* **do**
    Solve Eq. (6) and Eq. (7);
    Calculate numerical flow rate;
    Residual checking: Eq. (13);
    if $Residual > 0.5\%$ **then**
        Update K_z according to Eq. (12);
        Continue;
    else
        $K_z^{nu} \leftarrow K_z$;
        return K_z^{nu}
    end
end

(2) Discharge coefficient-based approach

A series of simulations is first performed to establish the characteristic performance map of the mold and determine the model parameter E in Eq. (11). Then the initial discharge coefficient C_d^0 is computed with the sample thickness and the initial permeability anisotropy α_g^0 using apparent transverse permeability:

$$\alpha_g^0 = \frac{\sqrt{K_x K_y}}{K_z^a} \tag{14}$$

The transverse permeability is then updated iteratively using the newly computed discharge coefficient $C_d(t, \alpha^i)$, following evaluation of residual R_{Cd}:

$$\alpha_g^i = \frac{\sqrt{K_x K_y}}{K_z^i} \tag{15}$$

$$R_{Cd} = \frac{K_z^i - K_z^{i-1}}{K_z^i} \times 100\% \tag{16}$$

This approach can greatly facilitate the post-processing of experimental data compared to the previous one. The performance of the test mold is obtained through an initial parametric study and no additional simulation is needed once the model parameter E is determined. The method is summarized in Algorithm 2 below.

Algorithm 2: C_d based approach

Input : K_x, K_y, K_z^a, h
Output : K_z^{Cd}
$\alpha^0 \leftarrow \frac{sqrt(K_x \times K_y)}{K_z^a}$;
$C_d^0 \leftarrow C_d(h, \alpha^0)$;
$i = 0$;
while *True* **do**
  $++i$;
  $K_z^i \leftarrow \frac{K_z^a}{C_d^{i-1}}$;
  $Residual \leftarrow$ Eq. (16);
  if $Residual > 0.5\%$ **then**
    $\alpha_i \leftarrow \frac{sqrt(K_x \times K_y)}{K_z^i}$;
    $C_d^i \leftarrow C_d(h, \alpha^i)$;
    Continue;
  else
    return $K_z^{Cd} = K_z^i$
  end
end

5.4 Validation

A 3D orthogonal glass textile TG96N (3250 g/m^2, Texonic Inc.) was characterized with the experimental setup to show the validity of the two iterative methods for anisotropic fibrous reinforcements. A first series of tests were conducted following the conventional method. As summarized in Table 2, four fiber volume fractions were considered by changing the cavity thickness while keeping the number of fabric layers constant. Each sample was weighted to evaluate the actual fiber volume fraction and each experiment was

repeated three times with fresh samples. Table 2 also shows the in-plane permeability along the warp and weft directions that were derived from the experimental results of Karaki et al. [26].

To validate the approach, a second series of tests were performed to measure directly the intrinsic permeability following the approach proposed by Huang et al. [6]. It consists of placing a highly permeable secondary Flow Distribution Layer (FDL) between perforated plates and sample. The FDL distributes fluid on the entire cross-section rapidly and create unidirectional flow in the tested specimen. However, some nesting is inevitable between the fibrous preform and the FDL so that the actual fiber volume fraction is reduced and the transverse permeability is overestimated. Huang et al. [6] characterized the nesting between the FDL and the preform by X-ray micro-computed tomography at different compaction levels. This analysis allowed relating the effective thickness of secondary FDL h_s (in millimeter) to the fiber volume fraction V_f through the following fitting function:

$$h_s = 3.49 \times 10^6 e^{-35.52 V_f} + 3.43 \times 10^{-1} \tag{17}$$

Note that Eq. (17) was obtained for a different type of woven fabric. However, the 3D fabric considered here possesses a similar compaction behavior and the experiments were conducted with the same secondary FDL as reported by Huang et al. As a first approximation, Eq. (17) was directly used in the present study without reproducing the Micro CT experiments and analysis.

Fig. 10 presents the apparent permeability of TG96N and its intrinsic permeability obtained following Huang's method and the two newly proposed approaches. Before correction, the permeability measured with secondary FDL is between 52% and 107% larger than the apparent permeability without secondary FDL (Fig. 10a). The former was overestimated due to the lower fiber volume fraction induced by nesting, while the latter was underestimated because of the presence of perforated plates. The data with secondary FDL was processed with Huang's method and presented in Fig. 10b as a reference value for validating the two iterative frameworks. As reported, the two iterative approaches yield nearly the same result, indicating they are equivalent. In addition, the intrinsic permeabilities obtained by the new approaches are quite close to those determined by Huang's approach. This strongly suggests that the two iterative approaches are valid.

Although Huang's method can eliminate the overestimation due to the nesting between sample and secondary FDL, one must first use volumetric imaging technology to obtain the model. Moreover, the model is expected to differ from one fabric or secondary FDL to another. Therefore, it can be expensive and time-consuming. This is another reason that motivates the development of the general approach reported in this work.

5.5 Sensitivity analysis

(1) Errors in in-plane permeability: In-plane permeability is a required input for the iterative algorithms. To mimic the measurement error of in-plane permeability, this analysis varied the in-plane permeability in a range of ± 20% while keeping transverse permeability constant in numerical identification. The investigation included two thickness levels (5 mm and 10 mm) and the global permeability anisotropy ranges from 1 to 100. The change in identified transverse permeability is less than 3% and decreases gradually as global permeability anisotropy increases. Considering typical textiles exhibit global permeability anisotropy ranging from 10 to 100, error in in-plane permeability shows only limited impact.

(2) Alignment of perforated plates: The numerical analyses presented so far assumes the upper and lower perforated plates are fully aligned. It is not always the case in practice. This could possibly modify the flow pattern within the sample. The holes in the perforated plates usually follow a hexagonal packing pattern to maximize the open space ratio, as illustrated in Fig. 2. The maximum misalignment angle is then considered as 30 degrees because of symmetry.

Two extreme conditions, i.e., the perfectly aligned and the 30° misaligned perforated plates, were investigated numerically with the proposed algorithm based on the experimental result of the reference porous medium. The transverse permeability identified is plotted in Fig. 11 as a function of the mass flow rate of the test liquid. Only 0.1% increase in the identified transverse permeability was obtained for the case with misaligned perforated plates. The authors tried to verify this experimentally but no difference could be observed.

6. Effect of test device on transverse permeability characterization

In this section, previous results obtained by two participants of Benchmark III [24] are re-analyzed to illustrate the usefulness of the correction method and the effect of test devices on transverse permeability characterization.

6.1 Mold description and analysis of performance

The setups used at Polytechnique Montreal (Fig. 2) and Wuhan University of Technology (Fig. 12) were investigated. The test principle is similar and both molds use perforated plates to control fiber volume fraction. However, some differences exist:

1) *geometry*: the diameter of the mold is 95.6 mm for Montreal and 114 mm for Wuhan.
2) *perforated plates*: the open space ratio of perforated plates in Montreal is 35.1% and 52.4% in Wuhan. The centroid distance between perforations is also different (see Fig. 2 and Fig. 12).
3) *pressure monitoring*: only one pressure sensor is mounted near the inlet for the mold in Montreal since fluid leaves the mold at atmospheric pressure. In contrast, one more pressure sensor was installed at outlet to monitor outflow pressure because the mold in Wuhan is closed with a top cover.

The characteristic performance map for the Wuhan device is presented in Fig. 12c. The minimum discharge coefficient is 59.2% ($t = 1.5$ mm, $\alpha = 1$), while it is 42.2% for the one in Montreal. The discharge coefficient of the device in Wuhan is constantly higher than that of the Montreal device (see Fig. 9 and Fig. 12c). This is consistent with the inherent difference in mold structure: the open space ratio of perforated plates in Wuhan is higher than that in Montreal (52.4% vs. 35.1%). It can be concluded that the Wuhan setup is more efficient. However, its discharge coefficient is still significantly lower than 1 for practical test conditions.

6.2 Permeability and measurement consistency

Experimental data from the two participants of Benchmark III were compared and reprocessed with the proposed approach. The textiles are non-crimp glass fabric produced by Saertex (NCF, 45°/90°/0°/45° of areal density 444 g/m^2) and twill glass woven fabric supplied by Hexcel (295 g/m^2). The in-plane permeability of the two fabrics was derived by polynomial fitting (see Table 4) from the results of Technische Universität Clausthal [33]. The test configurations are summarized in Table 3. Each test was repeated five times with fresh samples. Refer to [24] for more details on the benchmark materials and test guidelines.

The apparent and identified transverse permeability are plotted in Fig. 13a for the woven fabric and Fig. 13b for the non-crimp fabric. Only the identified permeability using the numerical-based approach is presented since the two iterative frameworks provide equivalent results. Fig. 13 shows that the apparent permeability of the two institutes is in good agreement. The values obtained by Wuhan tend to be higher but the difference is small considering the variability observed during the international benchmark. However, good repeatability does not necessarily mean the measured apparent permeability is accurate. Result shows that the identified permeability is significantly higher than apparent permeability. For woven fabrics tested in Montreal, the apparent permeability is 36.8%, 39.7%, and 45.8% lower than intrinsic values (for fiber volume fractions from low to high), while it is 28.3%, 29.8%, and 32.0% in Wuhan. For non-crimp fabric, the underestimation is 44.7%, 50.8%, 50.4% in Montreal and 34.6%, 36.3%, 34.3% in Wuhan. Overall, the amount of correction is higher for Montreal for all cases since the Wuhan setup possesses a larger open space ratio and is more efficient. It is also important to note that the number of plies (and hence thickness) was higher in Montreal which tends to increase the discharge coefficient. Additionally, it was observed that the correction is of greater importance for non-crimp fabric because of its low global permeability anisotropy.

To facilitate comparison, the apparent and identified permeability was adjusted to a nominal fiber volume fraction V_f using the following equation (derivation in Appendix A):

$$K_z^{V_f} = K_z^a \cdot \frac{{V_f^a}^2}{\left(1 - V_f^a\right)^3} \cdot \frac{\left(1 - V_f\right)^3}{{V_f}^2} \tag{18}$$

where V_f^a is the actual fiber volume fractions and $K_z^{V_f}$ the permeability for the nominal fiber volume fractions V_f. Three nominal fiber volume fractions are chosen here as the median values of the two institutes. They are 45%, 49%, and 53% for woven fabric and 46.8%, 50.5%, and 55% for non-crimp fabric. The apparent and identified permeability at nominal fiber volume fractions are presented in Fig. 14a for the woven fabric and Fig. 14b for the non-crimp fabric. The identified permeability is significantly improved in consistency. The maximum difference in average permeability of the woven fabric decreases from 18% (apparent permeability at $V_f^a = 53\%$) to 10% (between identified permeability). For the non-crimp fabric, the difference in apparent permeability is 4%, 9%, and 10% for the fiber volume fraction of 46.8%, 50.5%, and

55%. It decreases to 3%, 0.4%, and 0.6% after reprocessing. This again confirms the validity of the proposed algorithm in improving the consistency of transverse permeability measured with different devices. It also shows that geometrical differences in test molds may lead to apparently inconsistent results.

7. Conclusion

This study investigated the impact of flow distribution plates used in conventional 1D transverse permeability test devices for characterization of engineering textiles in saturated conditions. A general approach has been proposed to predict and model the performance of the test mold and correct the measured permeability value. Validation experiments were also conducted by measuring the intrinsic permeability of an isotropic reference porous medium and an anisotropic engineering textile. The key results are summarized as follows:

The underestimation of transverse permeability using the conventional unidirectional method was demonstrated experimentally for the first time by introducing a rigid reference porous medium. This effect was quantified by a dimensionless mold performance descriptor named discharge coefficient.

Using numerical simulation, the discharge coefficient was shown to depend on the geometry of the test device (open spaces in the flow distribution plates and cavity thickness) and on the anisotropy of the tested material. A simple analytical model was proposed to relate the mold performance to these key parameters.

An iterative framework was presented to identify the intrinsic transverse permeability from the conventional 1D test, either based on a series of numerical simulations or on the discharge coefficient model. The two approaches give equivalent results and agree well with the intrinsic permeability. The discharge coefficient approach is more promising as it reuses the performance map and no additional simulation is required.

The approach was finally applied to investigate the permeability discrepancy between two different molds. The discharge coefficient shows a strong positive correlation with the open space ratio of flow distribution plates. Permeability underestimation of the first mold is up to 46% for woven fabrics and 51% for non-crimp fabrics. In comparison, the second mold underestimates up to 32% and 36%, respectively. The iterative framework successfully improved the reproducibility of the two molds and eliminated underestimations.

Overall, the concept of discharge coefficient can be applied to any testing device based on 1D saturated flow and is promising for improving measurement consistency between different setups. It could be used to refine the analyses conducted during the recent benchmark that only considered the effect of perforated plate geometry and sample thickness separately [24]. Future investigations could also consider other types of distribution medium (such as honeycomb or sintered structures) to provide guidelines for highly efficient mold design.

Acknowledgments

This research was partially funded by the *Department of Mechanical Engineering* of Polytechnique Montreal and by the *Natural Sciences & Engineering Research Council of Canada* (NSERC) (Discovery Grant). Authors also gratefully acknowledge the financial support from the *Research Center for High Performance Polymer and Composite Systems* (CREPEC) and the "*Fonds de recherche du Québec - Nature et technologies*" (FRQNT). This research was also partially funded at Wuhan University of Technology by *Fundamental Research Funds for Central Universities* (2019-JL-003). Authors would like to express sincere thanks to Christian-Charles Martel and Steve Dube for their support in the laboratory.

Appendix A

Kozeny-Carman [34] model expresses the permeability as a function of fiber volume fraction V_f as follows:

$$K = \frac{{r_f}^2}{4k} \cdot \frac{\left(1 - V_f\right)^3}{{V_f}^2}$$

where r_f is fiber radius and k is Kozeny constant, which varies with V_f. The term $\frac{{r_f}^2}{4k}$ can be considered constant when the variation of V_f is limited to a small range. This gives the following equations for the actual and nominal fiber volume fractions V_f^a and V_f, and the corresponding permeability K_z^a and $K_z^{V_f}$:

$$K_z^a = \frac{{r_f}^2}{4k} \cdot \frac{\left(1 - V_f^a\right)^3}{{V_f^a}^2}, \quad K_z^{V_f} = \frac{{r_f}^2}{4k} \cdot \frac{\left(1 - V_f\right)^3}{{V_f}^2}$$

This leads to the correction equation Eq. (18).

References

[1] Rubino F, Carlone P. A semi-analytical model to predict infusion time and reinforcement thickness in VARTM and SCRIMP processes. Polymers (Basel). 2018;11(1).
[2] Joubaud L, Achim V, Trochu F. Numerical simulation of resin infusion and reinforcement consolidation under flexible cover. Polymer Composites. 2005;26(4):417-27.
[3] Darcy H. Public Fountains of The City of Dijon. 1856:1-9.

[4] Whitaker S. The method of volume averaging: Springer Science & Business Media; 1998.
[5] Arktas A. Survey of procedures in use for permeability measurements in liquid composite moulding processes. 2016.
[6] Huang W, Causse P, Hu H, Trochu F. Numerical and experimental investigation of saturated transverse permeability of 2D woven glass fabrics based on material twins. Polymer Composites. 2020;41(4):1341-55.
[7] Yang B, Huang W, Causse P, Béguin C, Wang J, Trochu F. On the design of test molds based on unidirectional saturated flows to measure transverse permeability in liquid composite molding. Polymer Composites. 2022.
[8] Kabachi MA, Stettler L, Arreguin S, Ermanni P. Concurrent characterization of through-thickness permeability and compaction of fiber reinforcements. Composites Part A: Applied Science and Manufacturing. 2021;141:106203.
[9] Willenbacher B, May D, Mitschang P. Metrological determination of inhomogeneous hydrodynamic compaction during unsaturated out-of-plane permeability measurement of technical textiles. Advanced Manufacturing: Polymer & Composites Science. 2019;5(2):51-4.
[10] Merhi D, Michaud V, Kampfer L, Vuilliomenet P, Manson JAE. Transverse permeability of chopped fibre bundle beds. Composites Part A: Applied Science and Manufacturing. 2007;38(3):739-46.
[11] Graupner R, Drechsler K. Quantitative transversal permeability testing-challenges and enhancements. Processdings of 14th FPCM. 2018.
[12] Li M, Gu YZ, Zhang ZG, Sun ZJ. A simple method for the measurement of compaction and corresponding transverse permeability of composite prepregs. Polymer Composites. 2007;28(1):61-70.
[13] Klunker F, Danzi M, Ermanni P. Fiber deformation as a result of fluid injection: modeling and validation in the case of saturated permeability measurements in through thickness direction. Journal of Composite Materials. 2015;49(9):1091-105.
[14] Li M, Wang SK, Gu YZ, Li YX, Potter K, Zhang ZG. Evaluation of through-thickness permeability and the capillary effect in vacuum assisted liquid molding process. Composites Science and Technology. 2012;72(8):873-8.
[15] Ouagne P, Breard J. Continuous transverse permeability of fibrous media. Composites Part A: Applied Science and Manufacturing. 2010;41(1):22-8.
[16] Barnett PR, Cook ZA, Hulett BM, Varma NH, Penumadu D. Influence of processing parameters on permeability and infiltration of compression molded discontinuous carbon fiber organosheet composites. Composites Part A: Applied Science and Manufacturing. 2022;152:106682.
[17] Willenbacher B, May D, Mitschang P. Out–of–plane capillary pressure of technical textiles. Composites Part A: Applied Science and Manufacturing. 2019;124(November 2018):105495-.
[18] Weitzenbock JR, Shenoi RA, Wilson PA. Measurement of three-dimensional permeability. Composites Part A: Applied Science and Manufacturing. 1998;29(1-2):159-69.
[19] Ahn SH, Lee WI, Springer GS. Measurement of the three-dimensional permeability of fiber preforms using embedded fiber optic sensors. Journal of Composite Materials. 1995;29(6):714-33.
[20] Nedanov PB, Advani SG. A method to determine 3D permeability of fibrous reinforcements. Journal of composite materials. 2002;36(2):241-54.
[21] Yun M, Sas H, Simacek P, Advani SG. Characterization of 3D fabric permeability with skew terms. Composites Part A: Applied Science and Manufacturing. 2017;97:51-9.
[22] Ballata WO, Walsh SM, Advani S. Determination of the transverse permeability of a fiber preform. Journal of reinforced plastics and composites. 1999;18(16):1450-64.
[23] Okonkwo K, Simacek P, Advani SG, Parnas RS. Characterization of 3D fiber preform permeability tensor in radial flow using an inverse algorithm based on sensors and simulation. Composites Part A: Applied Science and Manufacturing. 2011;42(10):1283-92.
[24] Yong AXH, Aktas A, May D, Endruweit A, Advani S, Hubert P, et al. Out-of-plane permeability measurement for reinforcement textiles: A benchmark exercise. Composites Part A: Applied Science and Manufacturing. 2021;148:106480.
[25] Scholz S, Gillespie JW, Heider D. Measurement of transverse permeability using gaseous and liquid flow. Composites Part A: Applied Science and Manufacturing. 2007;38(9):2034-40.
[26] Karaki M, Hallal A, Younes R, Trochu F, Lafon P. In-plane permeability prediction model for non-crimp and 3D orthogonal fabrics. Journal of the Textile Institute. 2018;109(8):1110-26.

[27] Fang L, Jiang J, Wang J, Deng C. Effect of Nesting on the Out-of-Plane Permeability of Unidirectional Fabrics in Resin Transfer Molding. Applied Composite Materials. 2015;22(3):231-49.
[28] Yang B, Wang S, Wang Y. Effect of Nesting in Laminates on the Through-Thickness Permeability of Woven Fabrics. Applied Composite Materials. 2018.
[29] Swery EE, Allen T, Comas-Cardona S, Govignon Q, Hickey C, Timms J, et al. Efficient experimental characterisation of the permeability of fibrous textiles. Journal of Composite Materials. 2016;50(28):4023-38.
[30] Studer J, Dransfeld C, Cano JJ, Keller A, Wink M, Masania K, et al. Effect of fabric architecture, compaction and permeability on through thickness thermoplastic melt impregnation. Composites Part A: Applied Science and Manufacturing. 2019;122:45-53.
[31] Roy T, Tan H, Pillai K. A Method to Estimate the Accuracy of 1-D Flow Based Permeability Measuring Devices. Journal of Composite Materials. 2007;41(17):2037-55.
[32] Patankar SV. Numerical heat transfer and fluid flow: CRC press; 1980.
[33] May D, Aktas A, Advani SG, Berg DC, Endruweit A, Fauster E, et al. In-plane permeability characterization of engineering textiles based on radial flow experiments : A benchmark exercise. Composites Part A: Applied Science and Manufacturing. 2019;121(March):100-14.
[34] Carman PC. Fluid flow through granular beds. Trans Inst Chem Eng. 1937;15:150-66.

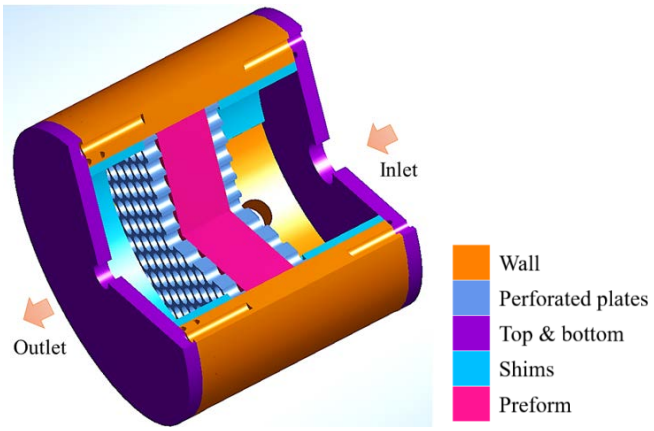

Fig. 1 Schematic diagram of a typical unidirectional transverse permeability test device.

(a) (b)

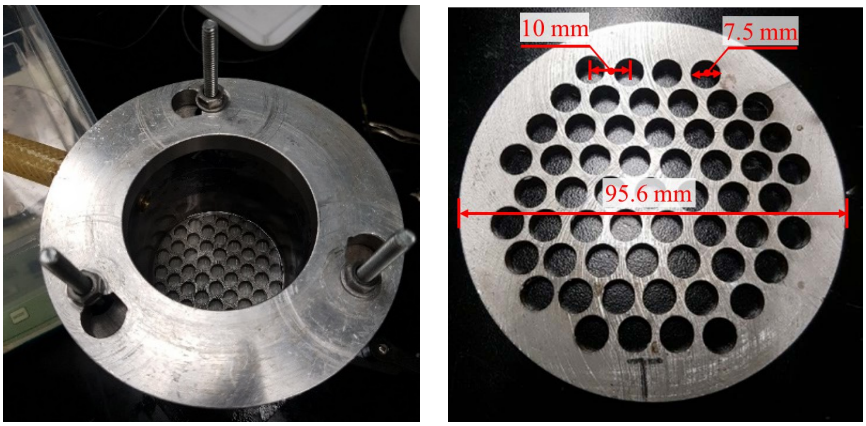

Fig. 2. Transverse permeability test mold at Polytechnique Montreal (a) and its perforated plate of 6.5 mm in thickness (b)

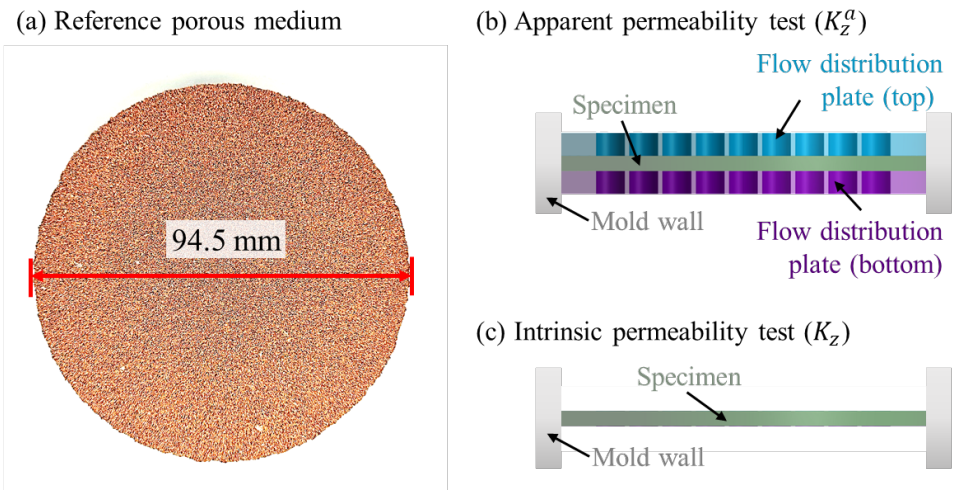

Fig. 3 Reference porous medium (a) and two test configurations: *apparent permeability test* with flow distribution plates (b) and *intrinsic permeability test* in freestanding conditions (c).

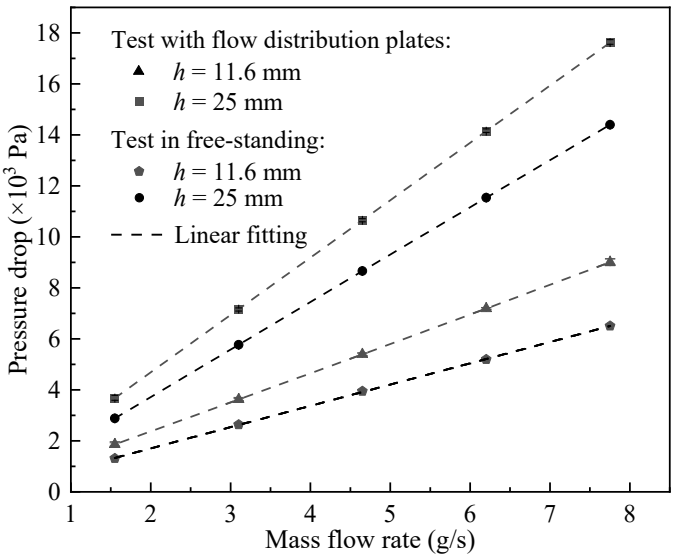

Fig. 4 Measured pressure drop across the thickness direction for the reference porous specimens with thickness (h) of 11.6 mm and 25 mm.

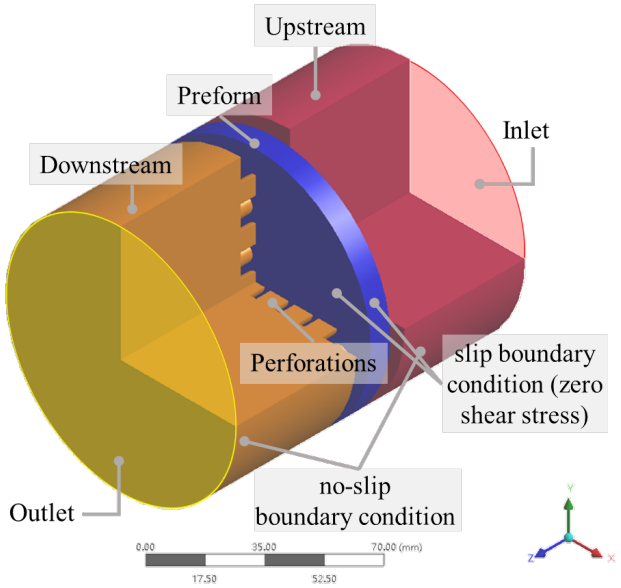

Fig. 5. Geometrical model and boundary conditions for 3D flow simulation.

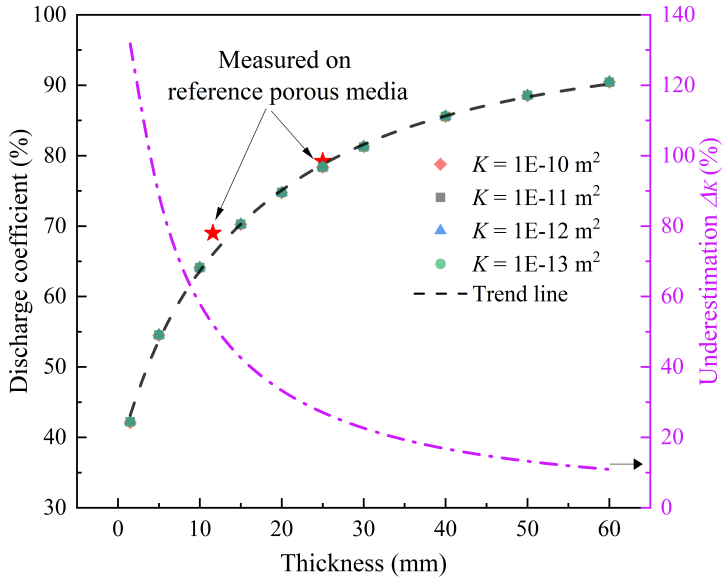

Fig. 6 Discharge coefficient (scatters) and transverse permeability underestimation for isotropic materials as a function of sample thickness for the test device shown in Fig. 2. Red stars indicate experimental measurements whereas all other markers correspond to numerical simulations

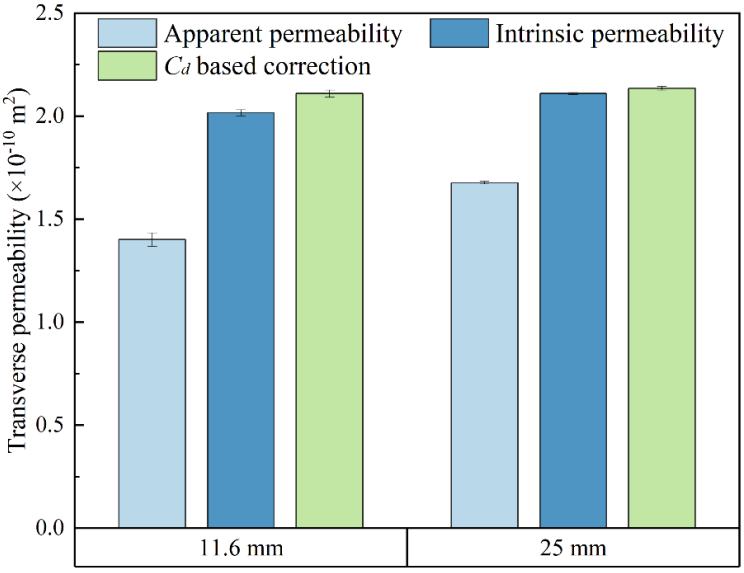

Fig. 7 Comparison of apparent, intrinsic, and identified transverse permeability based on numerically determined discharge coefficient for the reference porous medium.

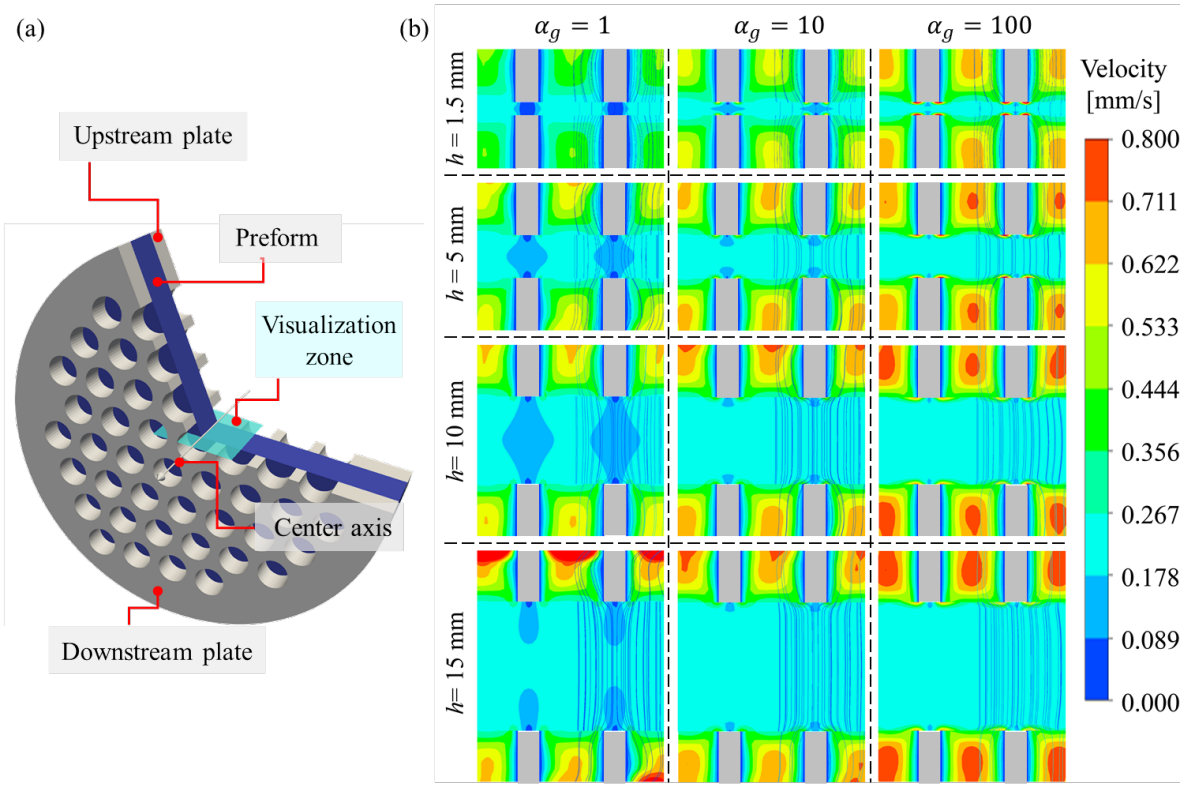

Fig. 8 Parametric investigation of fluid exchange through distribution plates for different preform thickness h and anisotropy α_g: the magnitude of intrinsic average velocity vector in the visualization zone of (a) is shown

in (b) superimposed with streamlines (only shown on the right half of each subplot). The gray color in (b) represents the solid part of perforated plates which is impermeable.

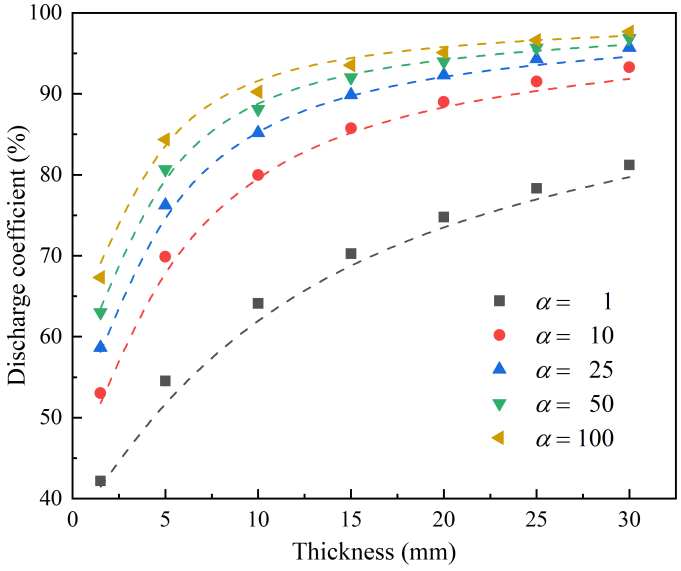

Fig. 9 Characteristic performance map for the mold presented in Fig. 2.

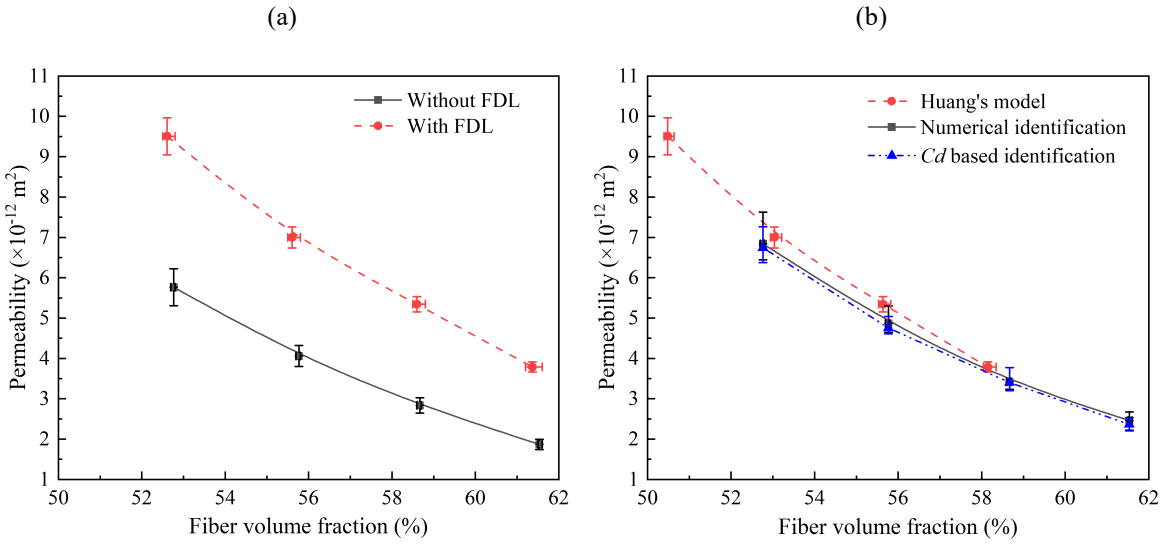

Fig. 10 Transverse permeability of TG96N: (a) raw data with and without secondary flow distribution layers; (b) corrected values with Huang's model and the two newly proposed iterative frameworks.

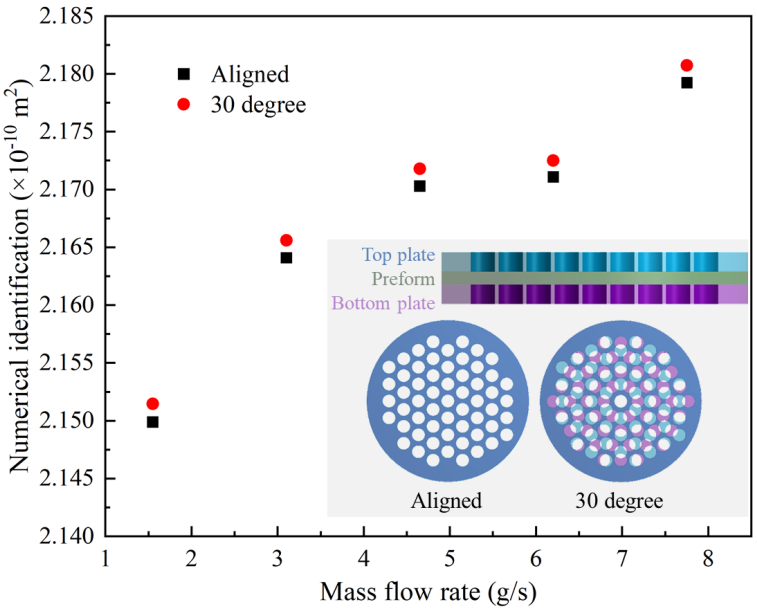

Fig. 11 Comparison of numerically identified permeability for aligned and not aligned perforated plates: two extreme conditions for hexagonal packing holes as depicted by the inset.

(a) (b)

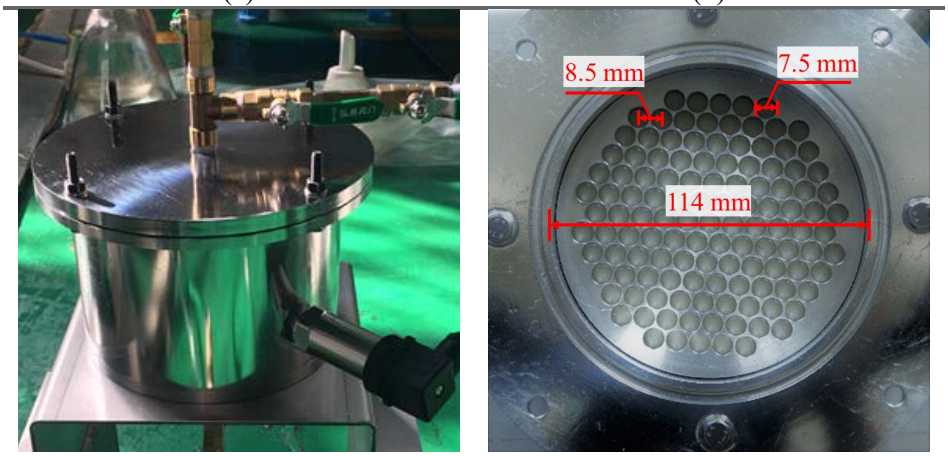

(c)

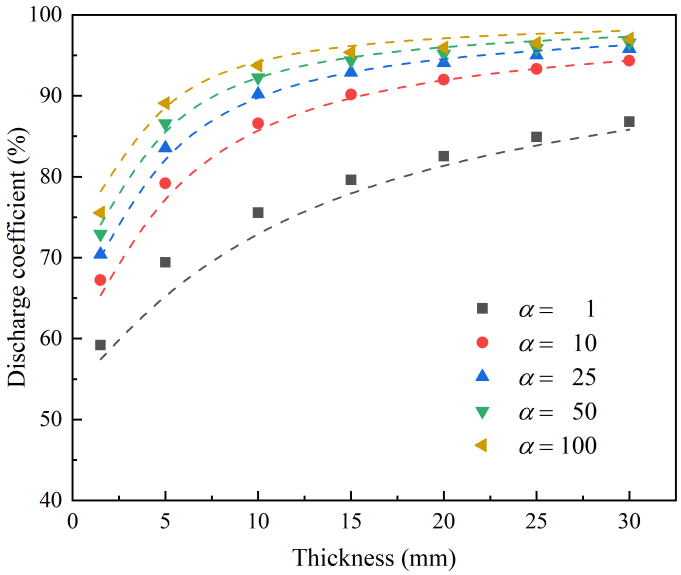

Fig. 12 Transverse permeability test mold of Wuhan University of Technology (a) and its perforated plate of 7 mm in thickness (b); Characteristic performance map of the mold (c).

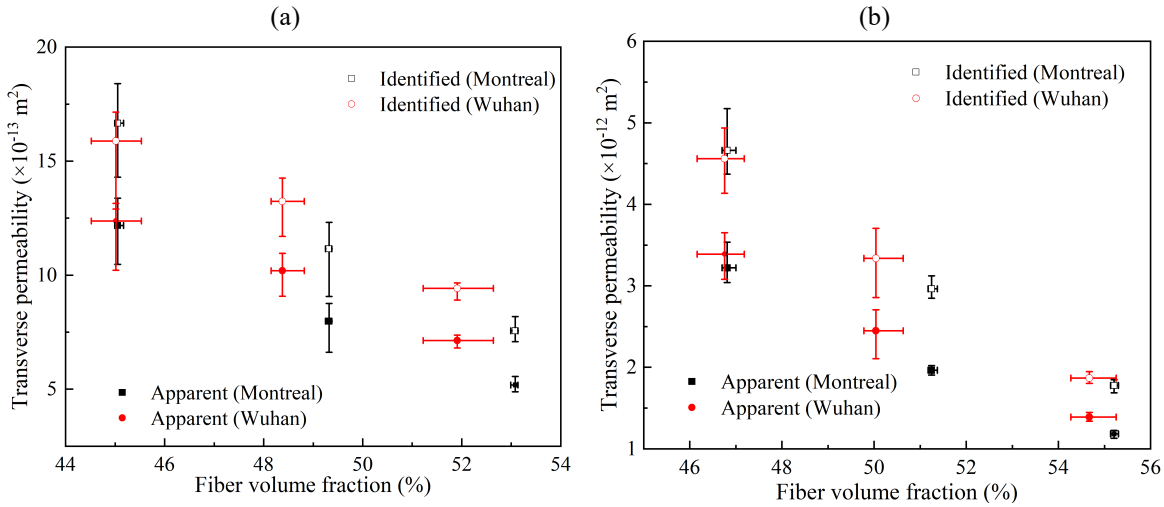

Fig. 13 The apparent and the identified permeability of (a) woven and (b) non-crimp fabric.

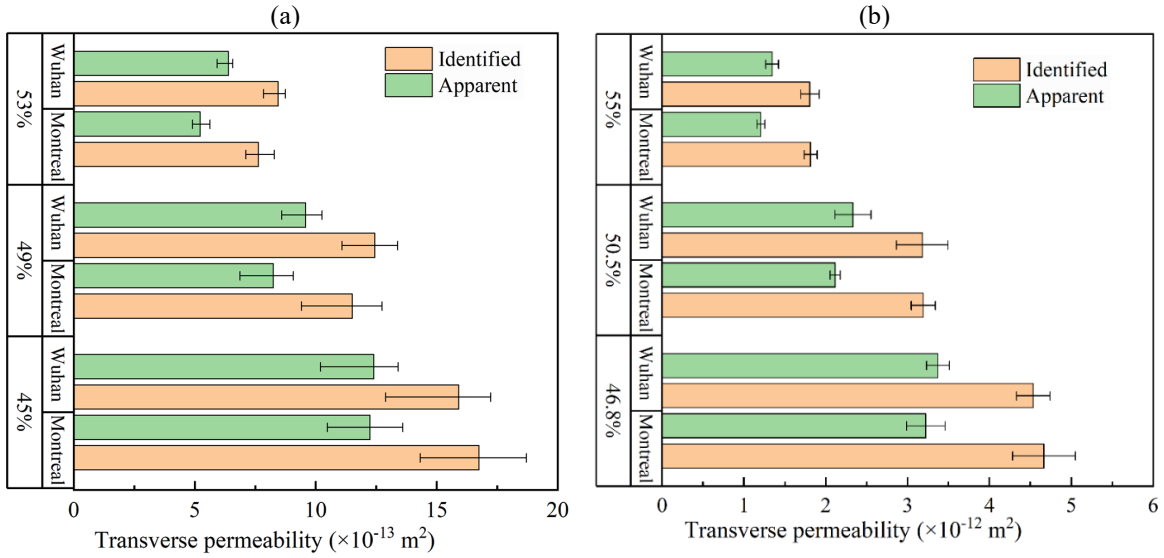

Fig. 14 The apparent and identified permeability of (a) woven fabric and (b) non-crimp fabric after being corrected to nominal fiber volume fractions.

Table 1 Transverse permeability of the reference porous medium

Sample thickness	Apparent permeability K_z^{a} $(\times 10^{-10}\ \mathrm{m}^2)$	Intrinsic permeability K_z $(\times 10^{-10}\ \mathrm{m}^2)$	Relative error $(K_z - K_z^{\mathrm{a}})/K_z^{\mathrm{a}}$
11.6 mm	1.41±0.030	2.02±0.015	43%
25.0 mm	1.67±0.027	2.11±0.005	26%

Table 2 Transverse permeability test configurations of TG96N

V_{f}	Without secondary FDL		With secondary FDL		In-plane permeability $(10^{-11}\ \mathrm{m}^2)$[26]	
	h (mm)	n	h (mm) *	n	K_x	K_y
53 %	9.45	4	10.58	4	14.2	7.0
56 %	8.94	4	10.08	4	11.2	4.54
59 %	8.49	4	9.64	4	8.36	2.62
62 %	8.10	4	9.23	4	5.74	1.25

* The thickness of the two layers secondary flow distribution layers is included.

Table 3 The transverse permeability test configurations for Benchmark III

Devices	Woven fabric			Non-crimp fabric		
	V_f	h (mm)	n	V_f	h (mm)	n
Polytechnique Montréal*	45. 1±0.06 %	5.29	21	46.8±0.10 %	5.29	14
	49.3±0.04 %	5.29	23	51.2±0.07 %	4.48	13
	53.1±0.06 %	4.48	21	55.2±0.08 %	4.48	14
Wuhan University of Technology	45.0±0.32 %	3.01	12	46.7±0.37 %	3.01	8
	48.4±0.24 %	3.01	13	50.0±0.31 %	2.80	8
	51.9±0.49 %	3.01	14	54.8±0.34 %	3.20	10

Note: All the benchmark tests in Montreal and Wuhan were performed without secondary flow distribution layers.

Table 4 In-plane permeability of the two benchmark fabrics

Non-crimp fabric			Woven fabric		
V_f	Permeability in 10^{-11} m^2		V_f	Permeability in 10^{-11} m^2	
46.8 %	K_x	5.54	45 %	K_x	6.56
	K_y	4.45		K_y	1.36
50.5 %	K_x	3.79	49 %	K_x	4.13
	K_y	2.99		K_y	0.64
55.0 %	K_x	2.15	53 %	K_x	2.61
	K_y	1.64		K_y	0.369